Contents lists available at ScienceDirect

Neurobiology of Disease

journal homepage: www.elsevier.com/locate/ynbdi

GRN−/− iPSC-derived cortical neurons recapitulate the pathological findings of both frontotemporal lobar degeneration and neuronal ceroidolipofuscinosis

Patrizia Bossolasco [a], Sara Cimini [b], Emanuela Maderna [b], Donatella Bardelli [a], Laura Canafoglia [c], Tiziana Cavallaro [d], Martina Ricci [b], Vincenzo Silani [a,e], Gianluca Marucci [b], Giacomina Rossi [b,*]

[a] *Department of Neurology and Laboratory of Neuroscience, Istituto Auxologico Italiano, IRCCS, Milan, Italy*
[b] *Unit of Neurology V and Neuropathology, Fondazione IRCCS Istituto Neurologico Carlo Besta, Milan, Italy*
[c] *Integrated Diagnostics for Epilepsy, Fondazione IRCCS Istituto Neurologico Carlo Besta, Milan, Italy*
[d] *Department of Neurosciences, Biomedicine, and Movement Sciences, University of Verona, Verona, Italy*
[e] *"Dino Ferrari" Center, Department of Pathophysiology and Transplantation, Università degli Studi di Milano, Milan, Italy*

ARTICLE INFO

Keywords:
Progranulin
Frontotemporal lobar degeneration
Neuronal ceroidolipofuscinosis
Induced pluripotent stem cells
Cortical neurons
Lysosomes
TDP-43
Fingerprints

ABSTRACT

Heterozygous mutations in the gene coding for progranulin (*GRN*) cause frontotemporal lobar degeneration (FTLD) while homozygous mutations are linked to neuronal ceroidolipofuscinosis (NCL). While both FTLD/NCL pathological hallmarks were mostly investigated in heterozygous *GRN*+/− brain tissue or induced pluripotent stem cell (iPSC)-derived neurons, data from homozygous *GRN*−/− condition are scarce, being limited to a postmortem brain tissue from a single case. Indeed, homozygous *GRN*−/− is an extremely rare condition reported in very few cases. Our aim was to investigate pathological phenotypes associated with FTLD and NCL in iPSC-derived cortical neurons from a *GRN*−/− patient affected by NCL. iPSCs were generated from peripheral blood of a *GRN* wt healthy donor and a *GRN*−/− patient and subsequently differentiated into cortical neurons. Several pathological changes were investigated, by means of immunocytochemical, biochemical and ultrastructural analyses. *GRN*−/− patient-derived cortical neurons displayed both TDP-43 and phospho-TDP-43 mislocalization, enlarged autofluorescent lysosomes and electron-dense vesicles containing storage material with granular, curvilinear and fingerprints profiles. In addition, different patterns in the expression of TDP-43, caspase 3 and cleaved caspase 3 were observed by biochemical analysis at different time points of cortical differentiation. At variance with previous findings, the present data highlight the existence of both FTLD- and NCL-linked pathological features in *GRN*−/− iPSC-derived cortical neurons from a NCL patient. They also suggest an evolution in the appearance of these features: firstly, FTLD-related TDP-43 alterations and initial NCL storage materials were detected; afterwards, mainly well-shaped NCL storage materials were present, while some FTLD features were not observed anymore.

Abbreviations: GRN, gene coding for progranulin; FTLD, Frontotemporal lobar degeneration; NCL, Neuronal ceroidolipofuscinosis; iPSCs, induced pluripotent stem cells; TDP-43, TAR-DNA binding protein-43; LAMP1, Lysosomal-associated membrane protein 1; TFEB, Transcription factor EB; PBMCs, Peripheral blood mononuclear cells; SCF, Stem cell factor; FTL-3, Fms-related tyrosine kinase ligand 3; KLF-4, Krüppel-like factor 4; OCT4, Octamer-binding transcription factor 4; Sox2, SRY-Box transcription factor 2; MOI, Multiplicity of infection; SSEA4, Stage-specific embryonic antigen-4; NGS, Normal goat serum; NSCs, Neural stem cells; NPCs, Neural progenitor cells; BDNF, Brain-derived neurotrophic factor; GDNF, glial cell derived neurotrophic factor; MAP2, Microtubule-associated protein 2; CUX1, cut like homeobox 1; PAX6, Paired box 6; TEM, Transmission electron microscopy; GRODs, Granular osmiophilic deposits.

* Corresponding author at: Unit of Neurology V and Neuropathology, Fondazione IRCCS Istituto Neurologico Carlo Besta, via Giovanni Amadeo 42, 20133 Milan, Italy.
E-mail address: giacomina.rossi@istituto-besta.it (G. Rossi).

https://doi.org/10.1016/j.nbd.2022.105891
Received 4 June 2022; Received in revised form 27 September 2022; Accepted 7 October 2022

1. Introduction

Mutations in the gene coding for progranulin (*GRN*) are linked to frontotemporal lobar degeneration (FTLD) (Baker et al., 2006; Cruts et al., 2006; Gass et al., 2006) and neuronal ceroidolipofuscinosis (NCL) (Smith et al., 2012). On one hand, heterozygous *GRN* mutations cause autosomal dominant FTLD, a group of heterogeneous degenerative dementias clinically characterized by behavioural frontotemporal dementia, primary progressive aphasia or corticobasal syndrome (Le Ber et al., 2008; Van Mossevelde et al., 2018). In patients younger than 65 years, FTLD is the second most common cause of degenerative dementia after Alzheimer's disease. The prevalence of FTLD was estimated about 10.8/100,000, while the incidence 1.61/100,000 person-years. The estimated lifetime risk is 1 in 742 (Coyle-Gilchrist et al., 2016). *GRN* pathogenic mutations explain 1–12% of FTLD and 4–26% of familial FTLD (Van Mossevelde et al., 2018).

On the other hand, homozygous *GRN* mutations give rise to NCL (CLN11), a lysosomal storage disorder affecting children and adults, characterized by ataxia, seizures and retinopathy (Canafoglia et al., 2014; Neuray et al., 2021). Incidence and prevalence rates are not available worldwide. Incidence rates are generally reported between 1 in 14,000 (Iceland) up to 1 in 100,000 (Gardner and Mole, 2021).

Very recently, the clinical spectrum associated with *GRN* mutations has been demonstrated to be wider than expected, with a few homozygous patients presenting frontotemporal dementia with visual signs (Huin et al., 2020).

From the neuropathological point of view, heterozygous *GRN* mutations cause abnormal accumulation and aggregation of the TAR DNA-binding protein 43 (TDP-43). In fact, TDP-43, localized in the nucleus under physiological conditions, gives rise to neuronal compact cytoplasmic inclusions and lentiform intranuclear inclusions in the affected cells (Neumann and Mackenzie, 2019).

After discovering the association between *GRN* mutations and NCL, markers of NCL pathology were searched for in FTLD *GRN* heterozygous patients, whereas homozygous were not available. Saposin D, subunit c of mitochondrial ATP synthase, the lysosomal proteins cathepsin D and lysosomal-associated membrane proteins LAMP1/2 were found to be elevated in brains of heterozygous patients, suggesting the existence of common pathological features between NCL and FTLD (Gotzl et al., 2014). In this line, phosphorylated and insoluble TDP-43 was found in few cases of non-*GRN* NCL (Gotzl et al., 2014).

Another pathological overlap between the two diseases was the finding, in few FTLD *GRN* heterozygous patients, of granular osmiophilic deposit-like material in brain cortex, storage material with a fingerprint profile pattern in lymphoblastoid cell lines (Ward et al., 2017) or electron dense material surrounded with rectilinear filaments in muscle (Terlizzi et al., 2017).

In induced pluripotent stem cells (iPSC)-derived cortical neurons from a FTLD *GRN* heterozygous patient, fingerprint-like and granular profiles were disclosed (Valdez et al., 2017).

Recently, the neuropathological examination of a *GRN* homozygous patient brain revealed the presence of lysosomal-associated deposits of curvilinear profiles with very few small fingerprints, and the absence of TDP-43 inclusions, although some abnormal immunoreactivity in cytoplasm was observed (Huin et al., 2020).

Progranulin is a growth factor involved in inflammation, wound healing and cancer (He et al., 2003; He and Bateman, 2003). In central nervous system, progranulin modulates inflammation and acts as a neurotrophic and neuroprotective factor (Van Damme et al., 2008; Ahmed et al., 2010; Toh et al., 2011; Tao et al., 2012; Tanaka et al., 2013). Progranulin was also shown to promote neurogenesis (Liu et al., 2021). Most mutations in progranulin are nonsense, splicing or frameshift and lead to a mutated mRNA which is degraded by the nonsense mediated decay mechanism (Behm-Ansmant et al., 2007). Such loss of function mechanism produces a condition of haploinsufficiency, associated with neurodegeneration due to reduced progranulin-mediated neuronal survival (Baker et al., 2006; Cruts et al., 2006).

Furthermore, increasing evidences indicate that progranulin has a role as lysosomal protein. *GRN* transcription is co-regulated with the transcription of other lysosomal genes by means of the transcription factor TFEB (Belcastro et al., 2011). Progranulin is delivered into lysosomes by its own sortilin receptor (Hu et al., 2010), as well as by physically interacting with prosaposin through the latter's receptors (Zhou et al., 2015). Within lysosomes, progranulin is cleaved by multiple cathepsins, in particular cathepsin L, to granulins peptides (Zhou et al., 2017a; Holler et al., 2017), and activates cathepsin D (Valdez et al., 2017; Zhou et al., 2017b; Beel et al., 2017). Progranulin affects also glucocerebrosidase activity either by direct interaction, according to some authors (Zhou et al., 2019), or through interaction with cathepsin D, which in turn regulates the levels of saposin C, an activator of glucocerebrosidase, according to others (Valdez et al., 2020).

Here, taking advantage from the availability of cells from one of very rare patients, we generated for the first time iPSC-derived cortical neurons from a *GRN*−/−homozygous NCL patient in order to study specific disease hallmarks, in particular the presence of cell storage material and abnormal behavior of disease-relevant proteins. In our *in vitro* model, we found pathological features including fingerprint profiles, lysosomal abnormalities and both TDP-43 and p-TDP-43 (p-TDP-43) abnormal deposits, covering the pathological spectrum from FTLD to NCL.

2. Materials and methods

2.1. Generation of induced pluripotent stem cells (iPSCs) and cortical neuron differentiation

This study was approved by the Ethics Committee of Fondazione IRCCS Istituto Neurologico Carlo Besta (n° 90;15/12/2021) and written informed consent was obtained from patient and healthy donors.

2.1.1. Sample collection and processing

Peripheral blood sample was collected from a patient affected by neuronal ceroidolipofuscinosis carrying the *GRN* Thr272fsX10 (NM_002087.4, c.813_816delCACT) homozygous mutation, referred to as *GRN*−/−, and from two age-matched *GRN* wild type (wt) healthy control subjects, a female and a male. The patient was a female aged 26 who began having recurrent convulsions at 23 years. Examinations revealed cerebellar ataxia and retinal dystrophy, and MRI disclosed cerebellar atrophy. She was firstly diagnosed as affected by NCL based on fingerprint findings on skin biopsy. For peripheral blood mononuclear cells (PBMCs) isolation, diluted blood samples were layered on a density gradient (1.077 g/ml) (Histopaque®-1077, Sigma-Aldrich, Merk KGaA, Darmstadt, Germany) and centrifuged. PBMCs were recovered from the plasma-density medium interface, washed and counted before reprogramming. In this study, we used two different clones derived from the *GRN*−/− patient and one clone/each from the two healthy donors. Six independent differentiations have been performed. The images presented in the manuscript are representative of one clone of the patient and one clone of a healthy donor.

2.1.2. Reprogramming of iPSCs

CytoTune®-iPS 2.0 Sendai Reprogramming Kit (Thermo Fisher Scientific, Waltham, MA, USA) was used for reprogramming PBMCs, following manufacturer's instructions. Briefly, 500.000 cells were cultured in StemPro-34 medium (Thermo Fisher Scientific, Waltham, MA, USA) supplemented with IL-3 (20 ng/ml), IL-6 (20 ng/ml), SCF (100 ng/ml) and FTL-3 ligand (100 ng/ml) (all from Gibco, Thermo Fisher Scientific, Waltham, MA, USA) for 4 days, and transduction was performed by adding the Klf4, Oct4, Sox2 and c-Myc virus, (KOS (Klf4–Oct3/4–Sox2) MOI = 5, hcMyc MOI = 5 and hKlf4 MOI = 3). Three days later, cells were transferred on hESC-Qualified matrigel-coated dishes (Corning, Glendale, Arizona, USA) in StemPro-34, and

thereafter medium was switched to iPSCs specific Essential 8 medium (Thermo Fisher Scientific, Waltham, MA, USA). When emerging colonies reached the appropriate size, they were picked and transferred on new matrigel-coated dishes for expansion. Each clone was characterized and differentiated after at least six passages using an EDTA 0.5mM solution.

2.1.3. Characterization of iPSCs clones

2.1.3.1. Karyotyping. Following an overnight exposition of the iPSCs clones to Colcemid solution (KaryoMAX™, Thermo Fisher Scientific, Waltham, MA, USA), chromosomes were stained with the fluorescent dye quinacrine mustard (Sigma-Aldrich, Merk KGaA, Darmstadt, Germany). Q-Band stained chromosomes were analysed.

2.1.3.2. The maintenance of GRN mutation. DNA was extracted by standard methods from the iPSCs, exon 7 of *GRN* was amplified by PCR using specific primers, bi-directionally sequenced using Big Dye Terminator v3.1 Cycle Sequencing Kit (Applied Biosystems, Thermo Fisher Scientific, Waltham, MA, USA) and analysed on a 3130xl Genetic Analyzer System (Applied Biosystems, Thermo Fisher Scientific, Waltham, MA, USA).

2.1.3.3. Stemness evaluation. Total RNA was isolated from iPSCs using Trizol Reagent (Thermo Fisher Scientific, Waltham, MA, USA) following manufacturer's instruction and RNA was reverse transcribed into cDNA using SuperScript II reverse transcriptase (Thermo Fisher scientific, Waltham, MA, USA). Briefly, after addition of Oligo(dt) (Eurofins Genomics), reaction was incubated at 42 °C for 40 min and 15 min at 70 °C. In order to assess the expression of the iPSCs specific markers, Sox 2, Oct 3/4 and Nanog, RT-PCR was then performed (denaturation 95 °C 30 s, annealing 60 °C 30 s, elongation 72 °C 1 min, for 35 cycles). Immunofluorescence analysis was performed on 4% paraformaldehyde (Santa Cruz Biotechnology, Dallas, Texas 75,220 USA) fixed coverslips. After 5 min of permeabilization with 0.3% Triton X-100 (Sigma-Aldrich, Merk KGaA, Darmstadt, Germany), cells were incubated with primary antibodies anti-TRA-1-60 (1:125, Invitrogen, Thermo Fisher scientific, Waltham, MA, USA), anti-SSEA4 (1:100, Invitrogen, Thermo Fisher scientific, Waltham, MA, USA) and anti-alkaline phosphatase (1:250, Abcam, Cambridge, UK) for 90 min at 37 °C in 10% Normal Goat Serum (NGS) (Gibco, Thermo Fisher Scientific, Waltham, MA, USA). After addition of Alexa 488 and Alexa 555 conjugated secondary antibodies for 45 min at room temperature (Invitrogen, Thermo Fisher scientific, Waltham, MA, USA), nuclei were counterstained using 4′,6-Diamidino-2-Phenylindole, Dihydrochloride (DAPI) (Sigma-Aldrich, Merk KGaA, Darmstadt, Germany). Confocal images were acquired with the Eclipse Ti inverted microscope (Nikon Eclipse C1, Tokyo, Japan).

2.1.3.4. In vitro spontaneous differentiation. To assess the *in vitro* capability of iPSCs clones to spontaneously differentiate into the three primordial germ layers (ectoderm, mesoderm and endoderm), iPSCs were seeded onto low adhesion plates in HuES medium (DMEM/F12, 20% knock-out serum replacement, 2 mM L-glutamine, 10 U/ml penicillin, 10 μg/ml streptomycin, 0.1 mM MEM NEAA, 110 μM β-mercaptoethanol) (all from Thermo Fisher Scientific, Waltham, MA, USA) for 7 days and the generated Embryoid bodies subsequently plated onto matrigel coated dishes in Essential 8 medium. The expression of specific markers β III tubulin for ectoderm, desmin for mesoderm, and alpha- fetoprotein for endoderm was evaluated by immunofluorescence using the respective antibodies (anti-β III tubulin, 1:500, Abcam, Cambridge, UK; anti-desmin, 1:10, Chemicon, Sigma-Aldrich, Merk KGaA, Darmstadt, Germany; anti-alpha-fetoprotein, 1:125, Invitrogen, Thermo Fisher scientific, Waltham, MA, USA).

2.1.4. Differentiation of iPSC-derived neural stem cells (NSCs)

Generation of NSCs from iPSCs was performed using the PSC Neural Induction Medium (Thermo Fisher Scientific, Waltham, MA, USA) following manufacturer's indication. Briefly, to iPSCs colonies at about 15–25% confluency pre-warmed complete PSC Neural Induction Medium was added and maintained for 7 day. The eighth day cells were harvested and expanded in pre-warmed complete Neural Expansion Medium on matrigel coated dishes. After at least 6 passages, positivity for the specific NSC marker Nestin (antibody anti-nestin 1:100, BD Biosciences) was evaluated by immunocytochemistry.

2.1.5. Differentiation of iPSCs into cortical neurons

iPSCs were differentiated into cortical neurons as previously described (Germain et al., 2014). Briefly, iPSC colonies at 60%–75% confluence were cultured in N2B27 medium (Neurobasal medium, 2% B27, 1% N2, 1% Insulin Transferrin Selenium, 2 mM L-Glutammine, P/S) (all reagents from Thermo Fisher Scientific, Waltham, MA, USA) supplemented with 500 ng/ml Noggin (R&D Systems, Minneapolis, MN, USA). After 10 to 20 days, the appearing neural rosettes were manually passaged on polylysine-laminin (Sigma-Aldrich, Merk KGaA, Darmstadt, Germany) coated dishes and cultured in the same medium for additional two weeks. N2B27 medium was then switched to Neural Differentiation Medium (Neurobasal medium, 2% B27, 1% NEAA, 2 mM L-Glutammine) (all reagents from Thermo Fisher Scientific, Waltham, MA, USA), with the addition of 10 ng/ml BDNF, 10 ng/ml GDNF (both from Peprotech, Thermo Fisher Scientific, Waltham, MA, USA), 1 μM Ascorbic Acid and 200 μM cAMP (both from Sigma- Aldrich, Merk KGaA, Darmstadt, Germany). One week later, the resulting neural progenitor cells (NPCs) were dissociated, plated at low density (1×10^5–1.5×10^5 cells) and not passaged any more until terminal differentiation.

2.1.6. Characterization of cortical neurons

Immunofluorescence analysis was performed as described for stemness evaluation, for the expression of both cortical neuron-specific markers and disease-related markers using the following primary antibodies: anti-SMI312 (1:1000, Covance, Labcorp, Burlington, North Carolina, USA), anti-β III tubulin (1:500, Abcam, Cambridge, UK), anti-MAP2 (1:200 Abcam, Cambridge, UK), anti-VGlut1 (1:50 Proteintech, Deansgate Manchester, United Kingdom), anti-CUX1 (1:200 Proteintech, Deansgate Manchester, United Kingdom), anti-LAMP1 (1:200 Proteintech, Deansgate Manchester, United Kingdom), anti-TDP-43 (1:500, Proteintech, Deansgate Manchester, United Kingdom), and anti-p-TDP-43 (1:150, Cosmobio, Tokyo, Japan).

2.2. Morphometric analysis of lysosomes

The size of lysosomal particles (identified by LAMP1 staining) was evaluated using ImageJ-win64 software. The Analyze Particles menu command was used setting 30–300 size particles in pixel and 0.2–1.00 for circularity. Lysosomes having an area between 30 and 300 pixels were considered as "large" lysosomes. The cut-off of 30 pixels was chosen arbitrarily based on the size of the majority of vesicles in the healthy donor-derived neurons, that was around 30 pixels. Three fields from 3 independent experiments were evaluated.

2.3. Western blot analysis

Western blots were performed on cortical neurons derived from one clone/each of two *GRN* wt healthy donors and from two clones of the *GRN*−/− patient. Three independent western blots were carried out for each analysis.

Cortical neurons were collected at 100- and 150-days post-differentiation and lysed in RIPA buffer (50 mM Tris-HCl pH 8, 150 mM NaCl, 5 mM EDTA, 1% NP-40, 0.5% sodium deoxycholate, 0.1% SDS) containing Protease Inhibitor Cocktail (Roche Diagnostics GmbH, Mannheim, Germany) and Phosphatase inhibitor Cocktail (Sigma Aldrich, Merk KGaA, Darmstadt, Germany). The samples were kept in ice for 15 min, sonicated in ice at 50% power for 45 s, kept 15 min in ice,

centrifuged at 13000 ×*g* 15 min at 4 °C and the supernatant was recovered. Protein concentration was determined with BCA assay (Thermo Fisher Scientific, Waltham, MA, USA) and 30 μg of total proteins were subjected to electrophoresis using Bolt 4–12% Bis-Tris gels (Thermo Fisher Scientific, Waltham, MA, USA) and transferred onto PVDF membranes (Thermo Fisher Scientific, Waltham, MA, USA). The membranes were incubated with the following primary antibodies: anti-caspase 3/p17/p19 (1:1000, Proteintech, Deansgate Manchester United Kingdom); anti-cleaved caspase-3 (Asp175) (1:1000, Cell Signaling Technology, Danvers, MA, USA); anti-TDP43 (1:2000, Proteintech, Deansgate Manchester United Kingdom). An anti-actin antibody (1:3000; Millipore, Burlington, MA, USA,) was used as control for loading. Immunoreactivity was visualized by chemiluminescence (GE Healthcare, Milan, Italy). Densitometric analysis was performed with QuantityOne software (Bio-Rad, Hercules, California, USA).

2.4. Ultrastructural analysis

Adherent neurons were harvested with Accutase - Enzyme Cell Detachment Medium (Thermo Fisher Scientific, Waltham, MA, USA) following manufacturer's indications and resuspended in Neural Differentiation Medium.

Cells were centrifuged at 500 rpm for 5 min, washed in PBS solution, centrifuged at 500 rpm for 5 min and then resuspended in 4 ml of 2.5% glutaraldehyde in PBS freshly prepared, for 1 h at 4 °C. After 3 washes in PBS, the cells were fixed in 1% osmium tetroxide in PBS for 1 h, dehydrated in ascending series of graded ethyl alcohols, embedded in epoxy resin for 24 h at room temperature and left to polymerize for 24 h at 70 °C. Semi-thin sections of about 0.5 to 1 μm were obtained and colored with Toluidine blue before being examined via a light microscope. Thin sections of about 70 nm were contrasted with heavy metals (uranyl acetate substitute and lead citrate) and were examined using transmission electron microscope (FEI Tecnai Spirit equipped with an Olympus Megaview G2 camera) at an accelerated voltage of 80 kV.

2.5. Statistical analysis

All statistical analyses were performed using GraphPad Prism Software. Unpaired, two-tailed Student's *t*-test or Mann Whitney test were used, for normal or not normal distributions, respectively (Kolmogorov Smirnov normality test). *P*-values less than 0.05 were considered significant.

3. Results

Reprogramming of PBMCs obtained from the *GRN*-/- patient and the *GRN* wt control subjects was performed and the derived iPSCs were differentiated into cortical neurons in order to investigate the effect of the mutation on neurodegeneration and lysosomal function.

3.1. Characterization of iPSCs clones

iPSCs obtained from the healthy donors and the patient had normal karyotype (data not shown) and expressed stemness specific markers by RT-PCR (Sox2, Oct3/4, Nanog) (Fig. S1A and S2A) and by immunofluorescence (alkaline phosphatase, SSEA4, TRA-1-60) (Fig. S1B and S2B). DNA sequencing confirmed the wild-type *GRN* genotype in healthy donor-derived iPSCs (Fig. S1C) and the presence of the *GRN* mutation in patient-derived cells (Fig. S2C). In addition, both clones were able to spontaneously differentiate into the three germ layers as demonstrated by expression of specific markers β III tubulin, alpha- fetoprotein and desmin (Fig. S1D and S2D).

3.2. Differentiation of iPSCs into neural stem cells (NSCs)

NSCs generated from both healthy donor-derived and patient-derived iPSCs were positive to the NSC specific marker nestin (Fig. 2D and E).

3.3. Differentiation of iPSCs into cortical neurons and characterization

No differences were observed regarding the differentiation potential of the healthy donor-derived and patient-derived iPSCs, with the appearance of typical neural rosettes around the fifteenth day of differentiation (Fig. S3A) displaying a positivity for the specific neuroectodermal stem cell markers Nestin and Pax6 (Fig. S3B). Following dissociation, cells differentiated into neural progenitors and subsequently in fully differentiated cortical neurons (Fig. S3C and S3D).

By immunocytochemistry, neurons expressed specific neuronal cortical markers such as MAP2 (microtubule-associated protein 2) and CUX1 involved into dendrite development and branching (Fig. 1A and B). Additionally, cortical neurons were positive for VGlut1 encoding for the vesicular transporter of glutamate, and pan-axonal neurofilament specific marker SMI312 (Fig. 1C and D). Neurons were kept in culture for about 100 or about 150 days.

3.4. TDP-43 protein is mislocalized and cleaved in GRN−/− cortical neurons

Since TDP-43 is known to be mislocalized from the nucleus to cytoplasm in brain neurons of heterozygous *GRN*+/− FTLD patients, to determine its localization in *GRN*-/- and wt cells we performed immunocytochemical study on iPSCs, NSCs and mature cortical neurons. While in iPSCs (Fig. 2A-C) and NSCs (Fig. 2D-F) TDP-43 immunoreactivity was mainly normally localized in the nucleus with no difference between *GRN*−/− and wt cells, in neurons the percentage of TDP-43 mislocalized in cytoplasm was significantly higher in *GRN*−/− than in wt cells (4,89% ± 0,3 vs 1,65 ± 0,2%; p<0,0001 (Fig. 2G-I). Eleven different fields were observed, with a total of about 1200 nuclei analysed. In addition, for *GRN*−/− neurons we observed some clusters of cells (in 4 out of the 11 fields observed) displaying more than 50% of cells with TDP-43 cytoplasmic mislocalization (Fig. 2J). None of those clusters were observed in the wt neurons.

As pathological TDP-43 fragments are detected in FTD and it has been demonstrated that activated (cleaved) caspase 3 may cut TDP-43 generating C-terminal fragments, we investigated the presence of TDP-43 fragments and of caspase 3, both full-length and activated, in 100- and 150-days cultured cortical neurons. Biochemical analysis showed the presence of cleaved TDP-43 in *GRN*−/− neurons, as fragments around 25, 35 and 37 kDa were detected (Fig. 3A), while in wt neurons only full-lenght TDP-43 was present. Caspase 3 analysis showed a statistically significant higher level of this protein in *GRN*−/− neurons ($p = 0.0079$) (Fig. 3B) and, more importantly, the presence of its activated (cleaved) form only in *GRN*−/− neurons (Fig. 3B). Cleaved caspase 3 is recognized by both antibody anti-caspase 3/p17/p19 (upper part of Fig. 3B) and antibody anti-cleaved caspase-3 (Asp175) (middle part of Fig. 3B). Surprisingly, in 150-day-cultured neurons only full-length TDP-43 could be observed and no cleaved caspase (Fig. 3C, D).

The phosphorylated form of TDP-43, p-TDP-43, is abundantly present in FTLD. Here, we performed p-TDP-43 specific immunocytochemistry on low density neurons, and found that while in wt neurons p-TDP-43 was within the nucleus (Fig. 4A, B), in *GRN*−/− neurons was mostly mislocalized to the cytoplasm (Fig. 4C, D). On the whole, these findings suggest the existence of FTLD-linked pathological features in neurons derived from a NCL patient.

3.5. Lysosomes have abnormal morphology in GRN−/− cortical neurons

As progranulin is also a lysosomal protein, its absence is expected to affect lysosome morphology and/or function. We examined the lysosomes by staining the intramembrane LAMP1 protein, and while in wt neurons the lysosomal staining was homogeneous suggesting the

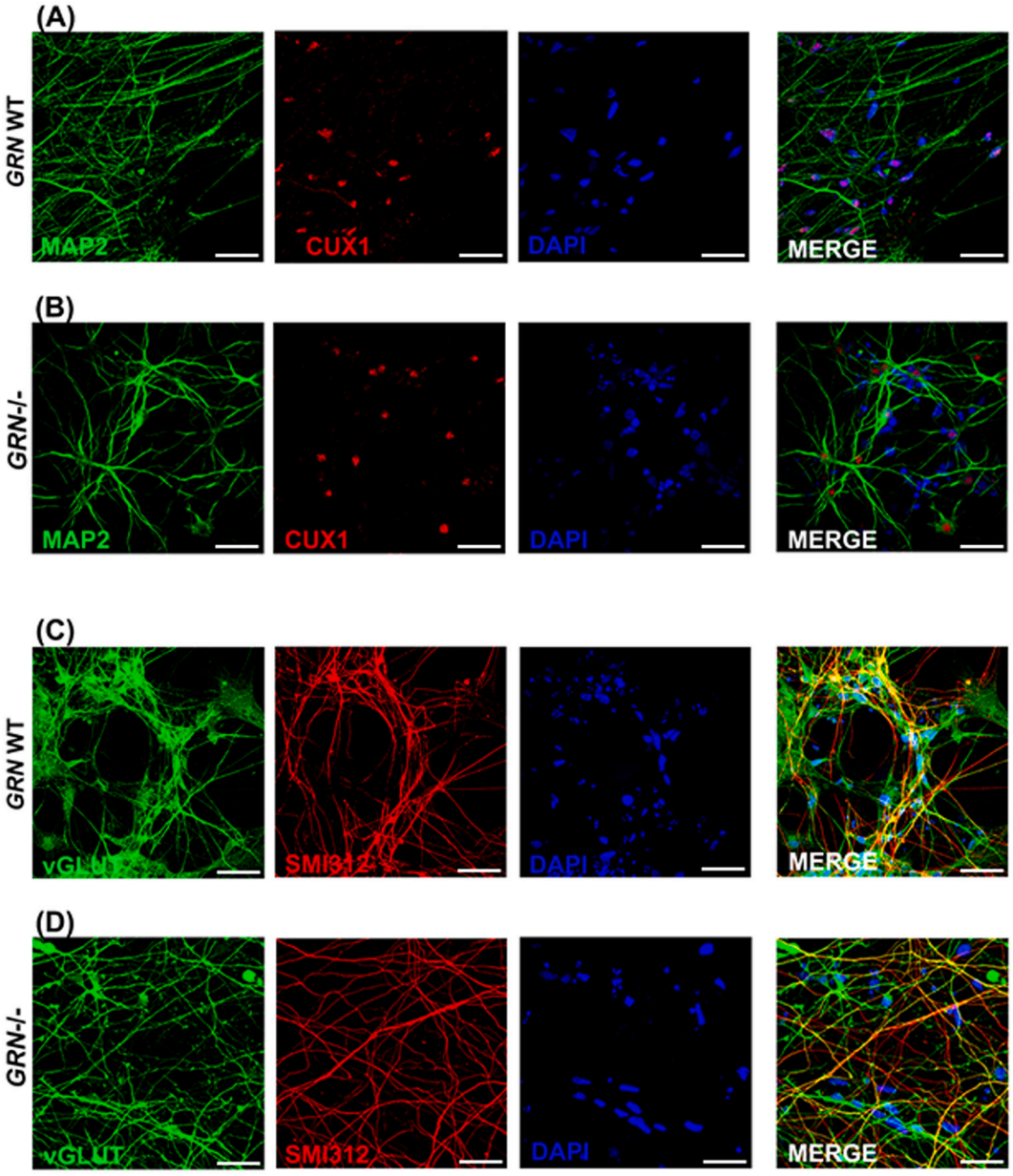

Fig. 1. Immunoflorescence of fully differentiated cortical neurons (100-days culture). *(A) GRN wt healthy donor-derived and (B) GRN−/− patient-derived cortical neurons expressing the cortical neuron markers MAP2 (green) and CUX1 (red). (C) GRN wt healthy donor-derived and (D) GRN−/− patient-derived cortical neurons expressing vGLUT1 and SMI312. Scale bar: 30 μm.*

presence of small normal organelles (Fig. 5A), within *GRN−/−* neurons we found large lysosomal structures, due to very large lysosomes (Fig. 5B). We evaluated the percentage of lysosomes having an area between 30 and 300 pixels (considered as "large" lysosomes) in wt and patient-derived cortical neurons. Three fields from 3 independent experiments were evaluated. The average number of large lysosomes in wt cells was significantly lower than in *GRN−/−* neurons (p = 0,0170). (Fig. 5C).

3.6. Storage material is present in GRN−/− cortical neurons

In NCL, lysosomal lipoproteic storage material gives rise to autofluorescence in hystochemical studies. In fact, we found autofluorescence in *GRN−/−* neurons and, by staining of LAMP1, showed that while no autofluorescence was seen in lysosomes from wt neurons (Fig. 5D), storage material was actually present within the lysosomes from *GRN−/−* neurons (Fig. 5E).

A structural definition of NCL storage material can be reached by means of ultrastructural study using transmission electron microscopy (TEM). Irregular granules heavy marked by the osmium tetroxide staining are defined as membrane-bound granular osmiophilic deposits (GRODs), while material with curved appearance is usually called curvilinear profiles; furthermore, membranes of lysosomal origin can be stacked in a very peculiar regular shape resembling fingerprints (for a review, Anderson et al., 2013).

While no storage material could be found in wt neurons (Fig. S4), 100-days cultured *GRN−/−*neurons showed GRODs (Fig. 6A-C), mixed curvilinear profiles (Fig. 6D), intermingled GRODs and parallel stacks of membranes forming small fingerprint profiles (Fig. 6E) and rare vesicles containing fingerprint profile patterns (Fig. 6F).

150-days cultured *GRN−/−* neurons disclosed a higher content of vesicles containing more organized fingerprint profiles (Fig. 7A-D).

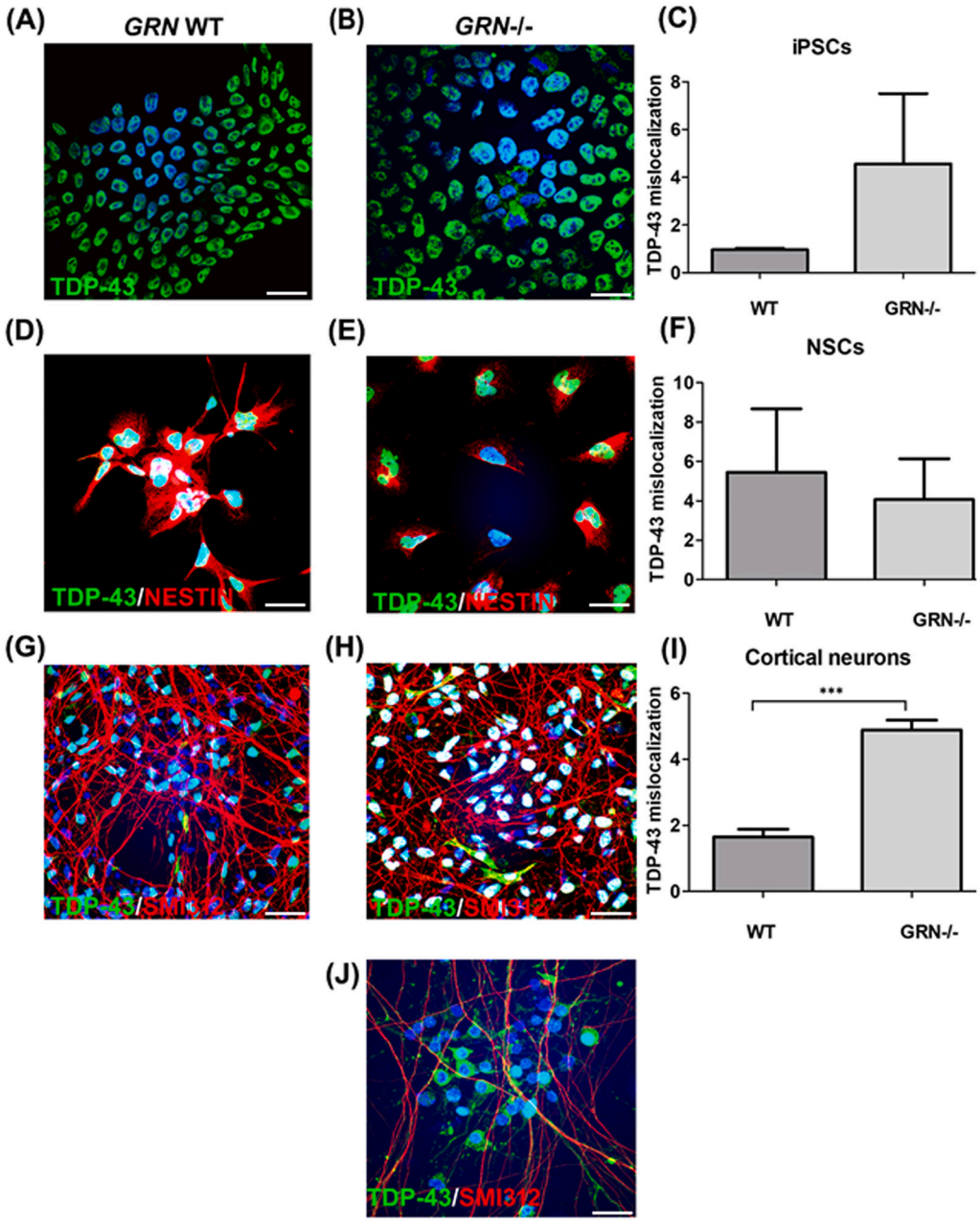

Fig. 2. Expression of TDP-43 in iPSCs (A-C), NSCs (D—F) and 100-days cultured cortical neurons (G-J). Immunofluorescence of TDP-43 (green) in (A) *GRN* wt healthy donor-derived and (B) *GRN*−/−patient-derived iPSCs. (C) Percentage of iPSCs. displaying a cytoplasmic mislocalization of TDP-43 in iPSCs. Immunofluorescence of TDP-43 (green) and NSCs specific marker Nestin (red) in (D) *GRN* wt healty donor-derived and (E) *GRN*−/− patient-derived NSCs. (F) Percentage of NSCs. displaying a cytoplasmic mislocalisation of TDP-43. Immunofluorescence of TDP-43 (green) and pan-axonal specific marker SMI312 (red) in (G) *GRN* wt healthy donor-derived and (H) *GRN*−/− patient-derived cortical neurons. (I) Percentage of cortical neurons displaying a cytoplasmic mislocalisation of TDP-43. (J) Immunofluorescence of a representative cluster from *GRN*−/− patient-derived cortical neurons, with high percentage of cytoplasmic mislocalization of TDP-43 (green), co-stained with the pan-axonal specific marker SMI312 (red). Scale bar: 30 μm.

Thus, these iPSC-derived neurons faithfully display NCL features.

4. Discussion

Progranulin, encoded by *GRN* gene, is a protein involved in inflammation, wound healing and cancer (Toh et al., 2011). In 2006, heterozygous mutations in *GRN* were discovered as causative of FTLD, opening an entirely new chapter in the study of neurodegenerative diseases (Baker et al., 2006; Cruts et al., 2006). FTLD includes a group of heterogeneous diseases pathologically characterized by deposition of tau, TDP-43 or FET proteins (Neumann and Mackenzie, 2019). Specifically, *GRN* mutations were associated with TDP-43 deposits. TDP-43 is a ubiquitous RNA binding protein physiologically present in the nucleus. In brains of FTLD patients carrying heterozygous *GRN* mutations, neuronal TDP-43 undergoes cytoplasmic mislocalization, insolubility, aggregation and post-translational modifications, such as phosphorylation, ubiquitination and cleavage (Buratti, 2018).

Surprisingly, in 2012 homozygous *GRN* mutations were disclosed as linked to a form of NCL (Smith et al., 2012). NCL are inherited progressive degenerative diseases that primarily affect the brain. They are considered lysosomal storage disorders, although peculiar, as exhibit heterogeneous and not disease-specific storage material (Kollmann et al., 2013). This material assumes different forms, often characteristically associated with the different NCL disorders (Anderson et al., 2013; Nita et al., 2016). As for the NCL named CLN11, caused by homozygous *GRN* mutation, fingerprint profiles were seen in lymphocytes and skin biopsy (Smith et al., 2012).

Since the discovery that *GRN* mutations cause both FTLD and NCL, several studies looked for common neuropathological features in these diseases. A high expression of NCL-related proteins was found in postmortem brains from *GRN* heterozygous patients (Gotzl et al., 2014), and some kind of storage material, GRODs-like and fingerprint-like, was detected in postmortem brain and lymphoblasts, respectively, from *GRN* heterozygous patients (Ward et al., 2017). Conversely, phosphorylated

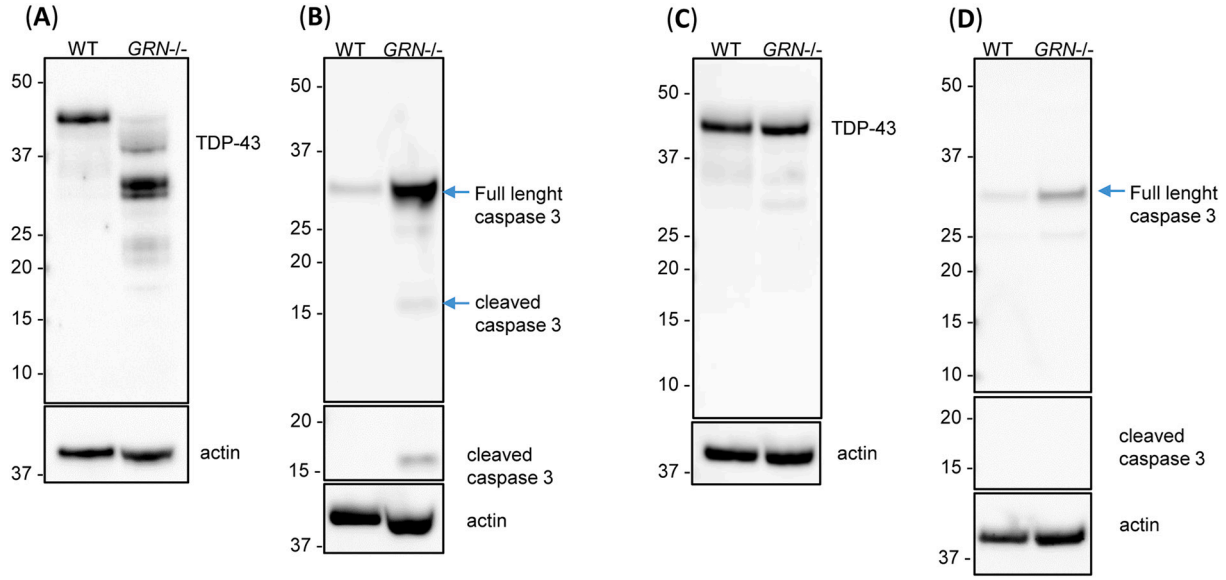

Fig. 3. Biochemical analysis of TDP-43 and caspase 3 by Western blotting (representative images). (A) TDP-43 and (B) full lenght and cleaved caspase 3, with respective actins as loading marker, after 100-days culture of *GRN* wt healthy donor-derived and *GRN*−/− patient-derived cortical neurons. Both anti-caspase 3/p17/p19 (upper panel) and anti-cleaved caspase-3 (Asp175) (middle panel) antibodies recognize cleaved caspase 3. (C) TDP-43 and (D) full lenght and cleaved caspase 3, with respective actins, after 150-days culture of *GRN* wt healthy donor-derived and *GRN*−/− patient-derived cortical neurons.

and insoluble TDP-43 was shown in NCL cases carrying a mutation in different genes from *GRN* (Gotzl et al., 2014).

Postmortem examination of brains from the very rare *GRN* homozygous patients affected by NCL (Huin et al., 2020) showed the presence of fingerprint storage material, as expected. However, the authors underlined the absence of TDP-43 cytoplasmic inclusions and of p-TDP-43, suggesting that TDP-43 pathology may only be associated with FTLD and not NCL phenotype.

Our hypothesis is that both storage material and TDP-43 pathology are present in *GRN*-related NCL and that the postmortem brain tissue, as a static condition, might not show the whole spectrum of pathological changes that could be showed in live neurons. Thus, thinking that this topic had to be better investigated, in particular the relationship between *GRN* homozygous mutations and the resulting pathology, we generated cortical neurons differentiated from iPSCs derived from PBMCs of a *GRN*−/− patient affected by NCL.

Cortical neurons differentiated from iPSCs obtained from a patient carrying a heterozygous *GRN* mutation had already been studied (Valdez et al., 2017), revealing decreased nuclear TDP-43, lipofuscin deposits, GRODs and some curvilinear profiles. In our *GRN*−/− cortical neurons, after 100-days culture, several kinds of pathological ultrastructural deposits were detected, such as GRODs, parallel stacks of membranes, mixed curvilinear profiles and rare fingerprint profiles. After a longer culture (150 days), the deposits appeared more numerous and well organized in the typical fingerprint profiles, suggesting a progressive deposition and reflecting the progressive nature of the pathology. Thus, while in heterozygous condition the storage material is less structured, homozygosity leads to a wider and more defined deposition, probably due to the more severe condition determined by the total absence of progranulin. Progranulin is also a protein with a lysosomal role. In fact, progranulin has been shown 1) to be processed to granulins by lysosomal enzymes (Zhou et al., 2017a; Holler et al., 2017); 2) to activate lysosomal protease cathepsin D (Valdez et al., 2017; Zhou et al., 2017b; Beel et al., 2017); 3) to affect the activity of lysosomal enzyme glucocerebrosidase (Zhou et al., 2019; Valdez et al., 2020). Progranulin absence affects lysosomal function, reflected by storage material engulfing lysosomes.

The relationship between progranulin haploinsufficiency and TDP-43 alterations has still to be clarified. One hypothesis is that lysosomal dysfunction hampers TDP-43 clearance (Gotzl et al., 2014), which in turn accumulate and forms cytoplasmic deposits, containing truncated and insoluble forms. Cells lacking progranulin have reduced autophagic flux, that may lead to accumulation of pathological forms of TDP-43 (Chang et al., 2017). One of the post-translational modifications of TDP-43 is the generation of C-terminal fragments, which are toxic (Igaz et al., 2009; Zhang et al., 2009). Several studies have tried to determine the origin of TDP-43 fragments and several explanations have been proposed, the proteolytic origin being the most studied (Buratti, 2018). Different proteolytic enzymes were investigated and caspase-3 in particular gave the most interesting results. The first evidence of 35 and 25 kDa TDP-43 fragments generated by activated caspase 3 was observed in cell models knock downed for progranulin (Zhang et al., 2007). Although other experiments on cell cultures failed to confirm this result and animal models of progranulin deficiency did not exhibit TDP-43 fragmentation (Dormann et al., 2009), the ability of activated caspase 3 to produce these fragments was demonstrated in an *in vivo* model of brain injury (Huang et al., 2017). Thus, we decided to concentrate our analysis on caspase 3. We found elevated levels of full-length caspase 3 in our *GRN*−/− cortical neurons, confirming previous data (Su et al., 2000). In addition, in our 100-days cultured *GRN*−/−cortical neurons we found activated caspase 3 and TDP-43 fragments; thus, we suggest that, in absence of progranulin, after 100-days culture, caspase 3 became activated and cut TDP-43 producing several fragments. We observed main fragments of about 35 kDa, and fragments of about 25 kDa and 37 kDa. Similar fragments have already been reported in studies on FTLD (Buratti, 2018; Arai et al., 2006; Neumann et al., 2009).

At variance, in 150-days neurons only full-length TDP-43 was observed as well as the absence of activated caspase 3. We only have a hypothesis concerning this aspect. We think that caspase 3 can activate early in a stress condition such as the absence of progranulin, leading to the cleavage of TDP-43. Accordingly, although in a different pathological background, caspase 3 has been demonstrated as an early event in patients affected by Alzheimer's disease (Cotman et al., 2005; Rissman et al., 2004).

However, if the stress condition prolongs and the storage material burden on lysosomes becomes the prevailing pathological condition, the activation of caspase 3 and the cleavage of TDP-43 is no longer required, and the intervention of some shutdown signal may be hypothesized. Our

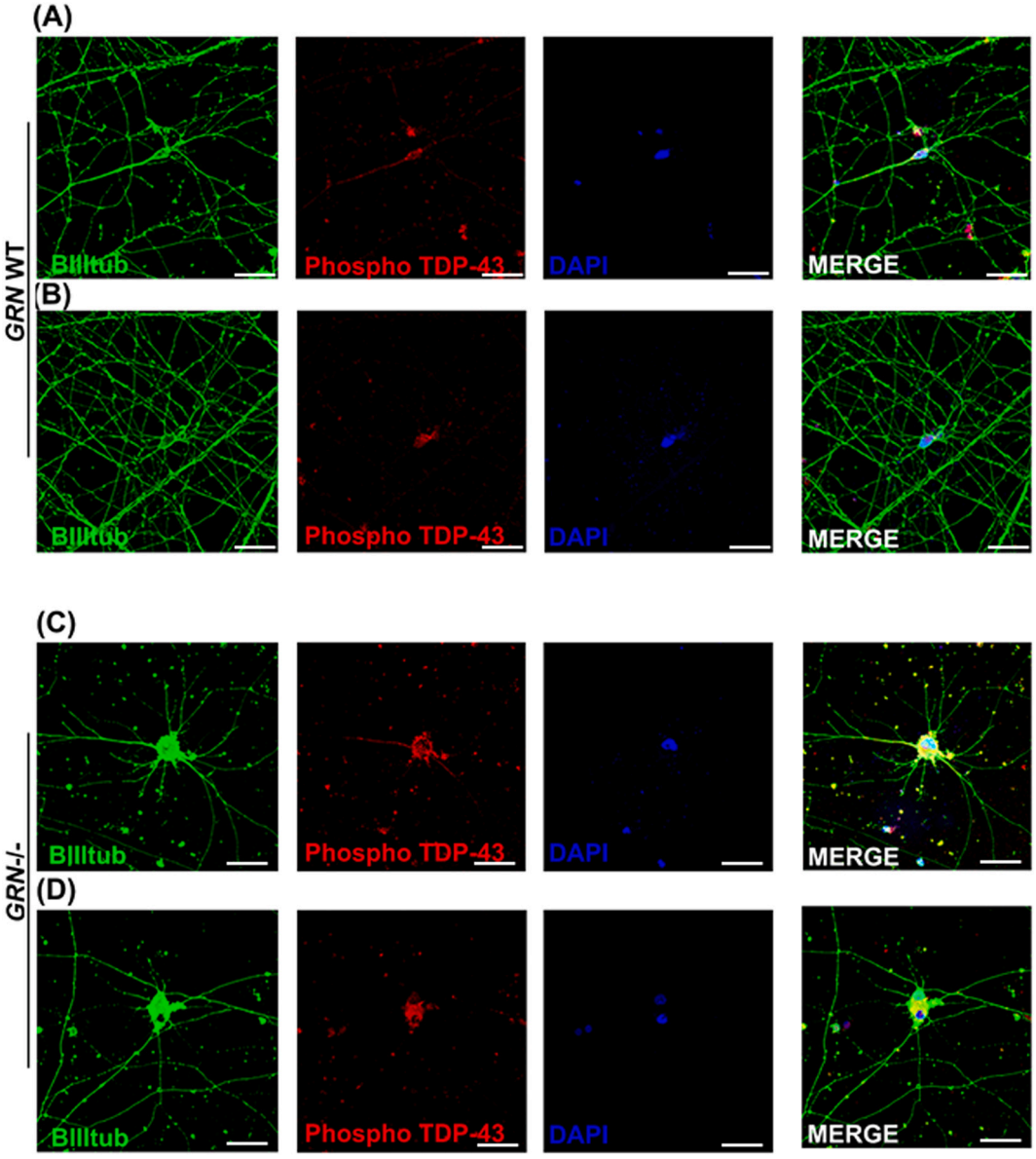

Fig. 4. Expression of p-TDP-43 in cortical neurons (100 days culture). *(A, B) Immunofluorescence of p-TDP-43 (red) and neuronal specific marker β III tubulin (green) in low density GRN wt healthy donor-derived cortical neurons. (C, D) Immunoflurescence of p-TDP-43 (red) and β III tubulin (green) in low density GRN−/− patient-derived cortical neurons. Scale bar: 30 μm.*

data support the view that at first the cells acquire the pathological hallmark of FTLD, i.e. altered TDP-43 and p-TDP-43 and their toxic fragments, mimicking the condition associated with heterozygous *GRN* mutations. However, the pathology then evolves towards an overwhelming lysosomal phenotype, while TDP-43 pathology subsides. This is in keeping with the neuropathological scenario of homozygous patients, where the TDP-43 pathology was scarce and no p-TDP-43 was found (Huin et al., 2020), and with our ultrastructural findings where more fingerprints were detected after 150-days of culture.

At variance with Huin (Huin et al., 2020), in our *GRN*−/− neurons after 100-days culture we found TDP-43 and p-TDP-43 cytoplasmic inclusions, clearly indicating that TDP-43 pathology is associated with *GRN* mutations independently from the zygosity. Very interestingly, in *GRN*−/− cultures, we observed clusters of neurons displaying more than 50% of cells with TDP-43 cytoplasmic mislocalization, while none of those clusters were observed in wt neurons. We think that these clusters are clones of neurons particularly vulnerable to the pathological process. It is possible that these neurons share functional features differentiating them from other less sensitive neurons. Mislocalized TDP-43 and p-TDP43, as well as autofluorescent and very large abnormal lysosomes, were disclosed in *GRN*−/− cortical neurons after 100-days culture by immunocytochemistry, while it was not possible to carry out these same evaluations after 150-days cultures, as overgrown neurons tended to detach from the slides, so that only electron microscopy on cell pellets and western blot on cell lysates were performed.

5. Conclusion

We produced a neuronal cell model which recapitulates the pathological hallmarks of both FTLD and NCL. Compared to postmortem brain tissue, it represents a dynamic model which allows to evaluate the temporal evolution of the pathology induced by *GRN* mutations. During the *in vitro* differentiation progression, that mimics the course of disease, we could observe that 1) high level of mislocalization of TDP-43 and p-TDP-43 was not present in iPSCs and NSCs, but only appeared in fully differentiated neurons; 2) TDP-43 can change from fragmented to full-

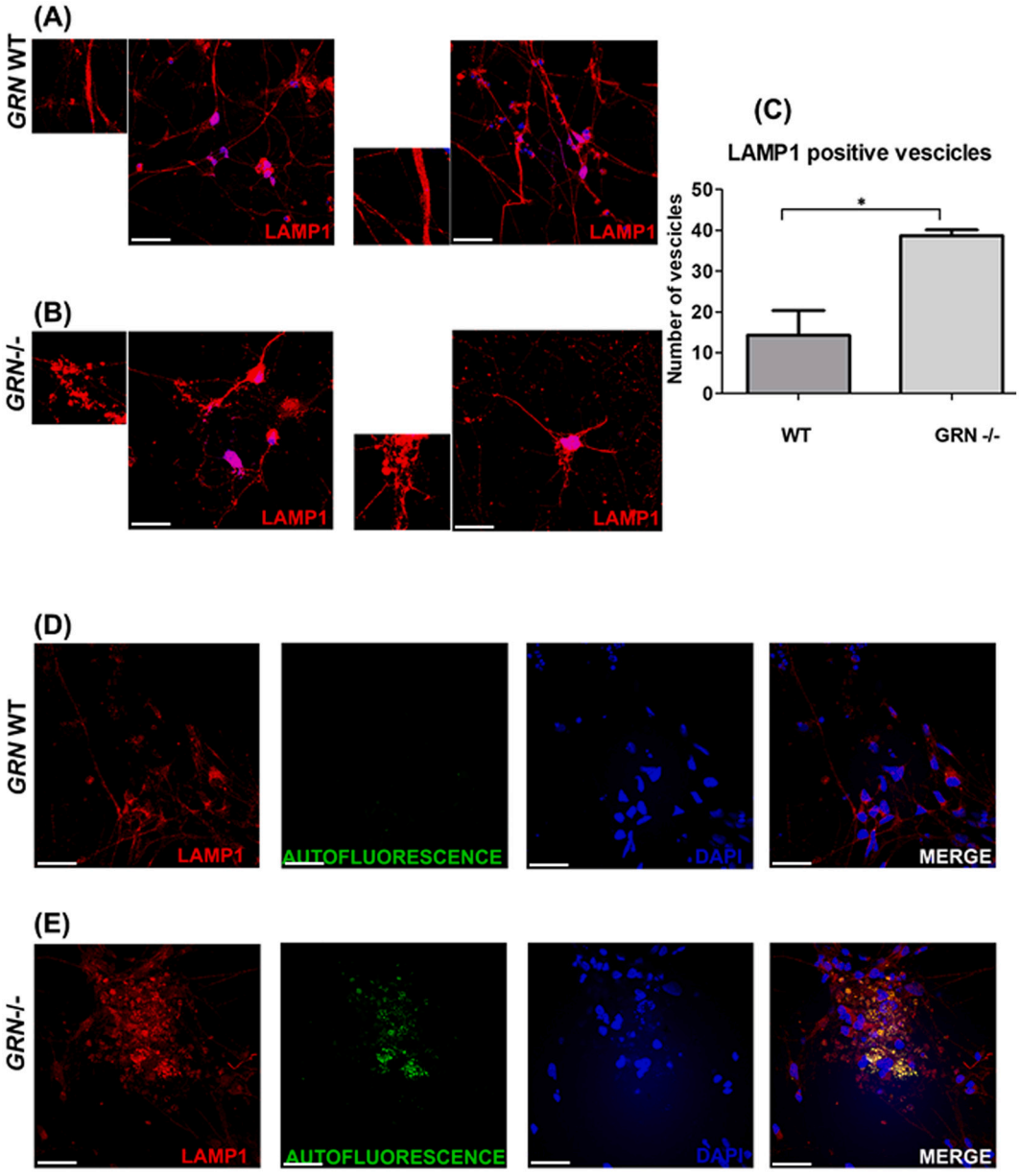

Fig. 5. Lysosome morphology characterization in cortical neurons (100 days culture). Immunofluorescence of the lysosomal membrane marker LAMP1 in (A) healthy donor-derived and (B) *GRN*−/− patient-derived cortical neurons. (C) Quantification of the number of vesicles with bigger size (area between 30 and 300 pixels). Immunofluorescence of LAMP1 and autofluorescent puncta in (D) healthy donor-derived and (E) *GRN*−/− patient-derived cortical neurons. Scale bar: 30 μm.

length forms, and caspase 3 can resume its inactive form; 3) lysosome storage material changes its shape to more diffused and best defined fingerprint profiles.

We are aware that one limitation of our study is the investigation of neurons derived from only a single subject. As a future direction, we will try to retrieve biological material from additional subjects, although we know that this condition is exceedingly rare. Furthermore, we think that investigation on additional proteolytic enzymes, besides caspase 3, able to generate TDP-43 fragments, as well as analysis of further lysosomal enzymes, besides cathepsin D and glucocerebrosidase, possibly affected by progranulin absence, should be perfomed.

Data availability

Raw Data that support the findings of this study are available from the corresponding author upon request and will be openly available on repositories at the Fondazione IRCCS Istituto Neurologico Carlo Besta and the Istituto Auxologico Italiano.

Ethical standards

All procedures were in accordance with the Helsinki Declaration. This study was approved by the Ethics Committee of the Fondazione IRCCS Istituto Neurologico Carlo Besta (n° 90;15/12/2021) and written informed consent was obtained from patient and healthy donors.

CRediT authorship contribution statement

Patrizia Bossolasco: Conceptualization, Methodology, Investigation. **Sara Cimini:** Investigation, Methodology. **Emanuela Maderna:** Formal analysis, Investigation. **Donatella Bardelli:** Investigation. **Laura Canafoglia:** Conceptualization. **Tiziana Cavallaro:** Supervision. **Martina Ricci:** Investigation. **Vincenzo Silani:** Supervision, Funding acquisition. **Gianluca Marucci:** Formal analysis. **Giacomina Rossi:**

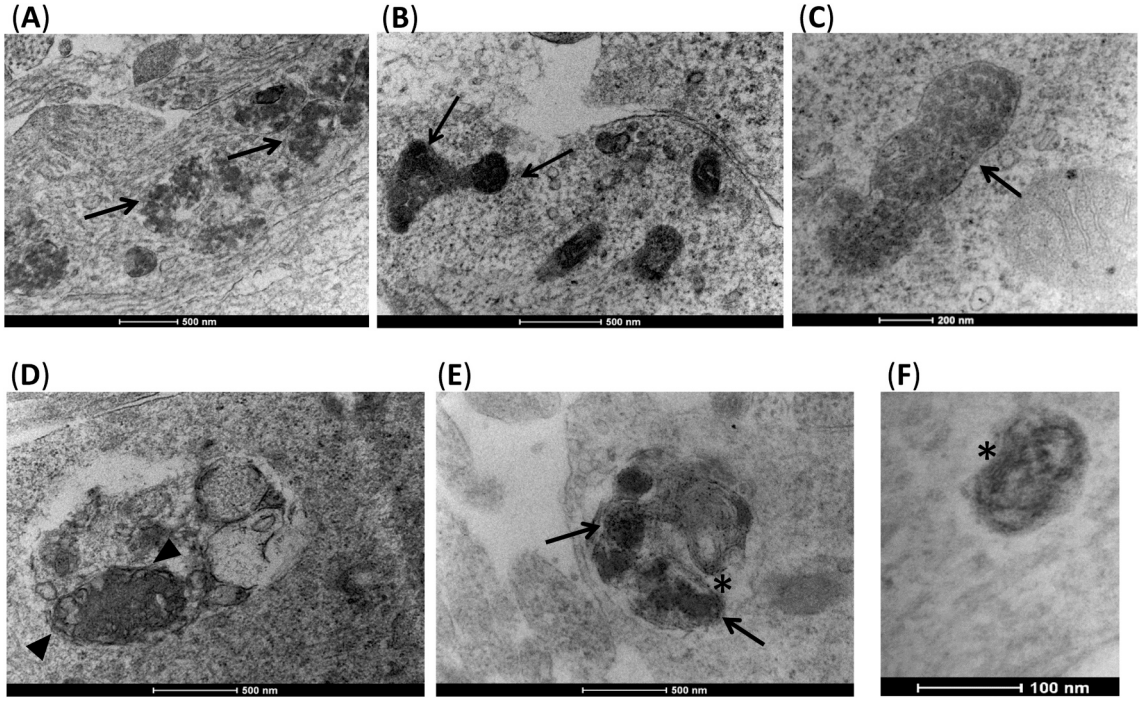

Fig. 6. Ultrastructural images of *GRN*−/− patient-derived cortical neurons after 100-days culture. (A-C) Membrane-bound granular osmiophilic deposits (GRODs, arrows). (D) mixed curvilinear profiles (arrowheads). (E) Intermingled GRODs (arrows) and parallel stacks of membranes forming small fingerprint profiles (asterisk). (F) A vesicle containing fingerprint profiles (asterisk).

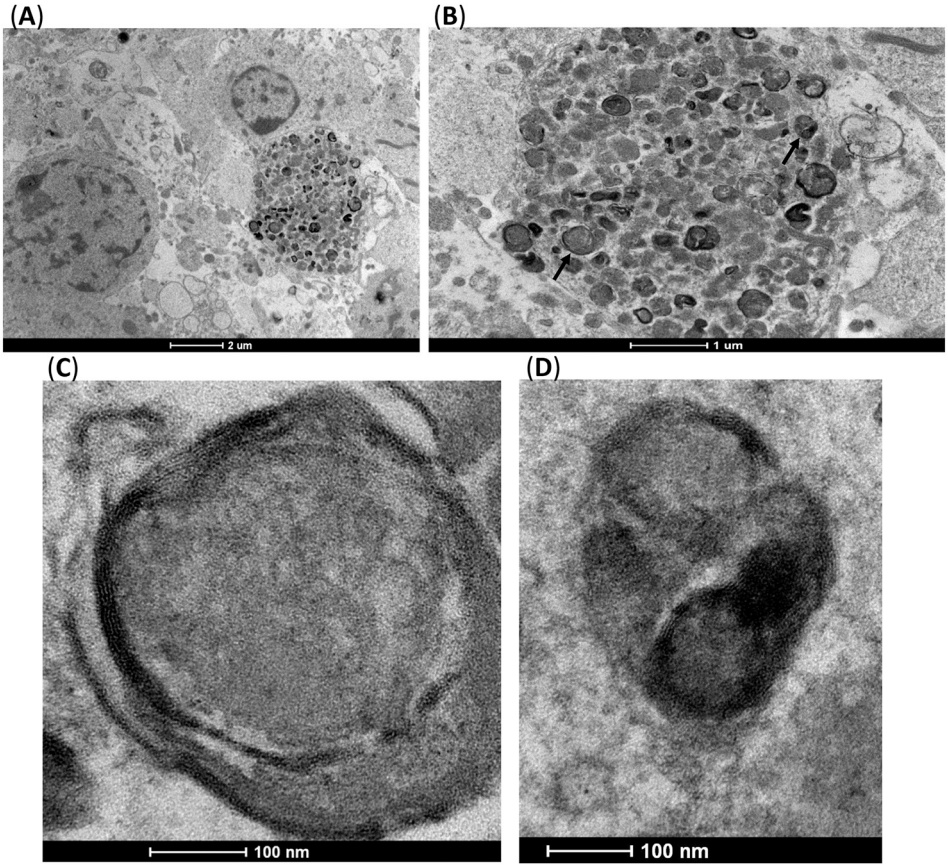

Fig. 7. Ultrastructural images of *GRN*−/− patient-derived cortical neurons after 150-days culture. (A, B) Neurons at low magnification, showing a high number of electron dense inclusions. (C, D) Higher magnification of the inclusions indicated by the arrows, showing fingerprint profiles.

Conceptualization, Writing – original draft, Writing – review & editing, Supervision, Funding acquisition.

Declaration of Competing Interest

The authors declare that the research was conducted in the absence of any commercial or financial relationships that could be construed as a potential conflict of interest.

Data availability

Data will be made available on request.

Acknowledgements

This work was supported by the Italian Ministry of Health: Ricerca Corrente RRC 2018-2021; RF-2013-02355764, C9GenALSPhen.

Appendix A. Supplementary data

Supplementary data to this article can be found online at https://doi.org/10.1016/j.nbd.2022.105891.

References

Ahmed, Z., Sheng, H., Xu, Y.F., et al., 2010. Accelerated lipofuscinosis and ubiquitination in granulin knockout mice suggest a role for progranulin in successful aging. Am. J. Pathol. 177 (1), 311–324.
Anderson, G.W., Goebel, H.H., Simonati, A., 2013. Human pathology in NCL. Biochim. Biophys. Acta 1832 (11), 1807–1826.
Arai, T., Hasegawa, M., Akiyama, H., et al., 2006. TDP-43 is a component of ubiquitin-positive tau-negative inclusions in frontotemporal lobar degeneration and amyotrophic lateral sclerosis. Biochem. Biophys. Res. Commun. 351 (3), 602–611.
Baker, M., Mackenzie, I.R., Pickering-Brown, S.M., et al., 2006. Mutations in progranulin cause tau-negative frontotemporal dementia linked to chromosome 17. Nature. 442 (7105), 916–919.
Beel, S., Moisse, M., Damme, M., et al., 2017. Progranulin functions as a cathepsin D chaperone to stimulate axonal outgrowth in vivo. Hum. Mol. Genet. 26 (15), 2850–2863.
Behm-Ansmant, I., Kashima, I., Rehwinkel, J., Saulière, J., Wittkopp, N., Izaurralde, E., 2007. Mrna quality control: an ancient machinery recognizes and degrades mrnas with nonsense codons. FEBS Lett. 581 (15), 2845–2853.
Belcastro, V., Siciliano, V., Gregoretti, F., et al., 2011. Transcriptional gene network inference from a massive dataset elucidates transcriptome organization and gene function. Nucleic Acids Res. 39 (20), 8677–8688.
Buratti, E., 2018. TDP-43 post-translational modifications in health and disease. Expert Opin. Ther. Targets 22 (3), 279–293.
Canafoglia, L., Morbin, M., Scaioli, V., et al., 2014. Recurrent generalized seizures, visual loss, and palinopsia as phenotypic features of neuronal ceroid lipofuscinosis due to progranulin gene mutation. Epilepsia. 55 (6), e56–e59.
Chang, M.C., Srinivasan, K., Friedman, B.A., et al., 2017. Progranulin deficiency causes impairment of autophagy and TDP-43 accumulation. J. Exp. Med. 214, 2611–2628.
Cotman, C.W., Poon, W.W., Rissman, R.A., Blurton-Jones, M., 2005. The role of caspase cleavage of tau in Alzheimer disease neuropathology. J. Neuropathol. Exp. Neurol. 64 (2), 104–112.
Coyle-Gilchrist, I.T.S., Dick, K.M., Patterson, K., et al., 2016. Prevalence, characteristics, and survival of frontotemporal lobar degeneration syndromes. Neurology. 86, 1736–1743.
Cruts, M., Gijselinck, I., van der Zee, J., et al., 2006. Null mutations in progranulin cause ubiquitin-positive frontotemporal dementia linked to chromosome 17q21. Nature. 442 (7105), 920–924.
Dormann, D., Capell, A., Carlson, A.M., et al., 2009. Proteolytic processing of TAR DNA binding protein-43 by caspases produces C-terminal fragments with disease defining properties independent of progranulin. J. Neurochem. 110 (3), 1082–1094.
Gardner, E., Mole, S., 2021. The genetic basis of phenotypic heterogeneity in the neuronal ceroid lipofuscinoses. Front. Neurol. 12, 754045.
Gass, J., Cannon, A., Mackenzie, I.R., et al., 2006. Mutations in progranulin are a major cause of ubiquitin-positive frontotemporal lobar degeneration. Hum. Mol. Genet. 15 (20), 2988–3001.
Germain, N.D., Chen, P.F., Plocik, A.M., et al., 2014. Gene expression analysis of human induced pluripotent stem cell-derived neurons carrying copy number variants of chromosome 15q11-q13.1. Mol Autism. 5 (1), 44.
Gotzl, J.K., Mori, K., Damme, M., et al., 2014. Common pathobiochemical hallmarks of progranulin-associated frontotemporal lobar degeneration and neuronal ceroid lipofuscinosis. Acta Neuropathol. 127, 845–860.
He, Z., Bateman, A., 2003. Progranulin (Granulin-epithelin precursor, pc-cell-derived growth factor, acrogranin) mediates tissue repair and tumorigenesis. J Mol Med (Berl). 81 (10), 600–612.
He, Z., Ong, C.H.P., Halper, J., Bateman, A., 2003. Progranulin is a mediator of the wound response. Nat. Med. 9 (2), 225–229.
Holler, C.J., Taylor, G., Deng, Q., Kukar, T., 2017. Intracellular proteolysis of progranulin generates stable, lysosomal granulins that are haploinsufficient in patients with frontotemporal dementia caused by grn mutations. eNeuro. 4 (4). ENEURO.0100-17.2017.
Hu, F., Padukkavidana, T., Vægter, C.B., et al., 2010. Sortilin-mediated endocytosis determines levels of the frontotemporal dementia protein, progranulin. Neuron. 68 (4), 654–667.
Huang, C.Y., Lee, Y.C., Li, P.C., et al., 2017. TDP-43 proteolysis is associated with astrocyte reactivity after traumatic brain injury in rodents. J. Neuroimmunol. 313, 61–68.
Huin, V., Barbier, M., Bottani, A., et al., 2020. Homozygous GRN mutations: new phenotypes and new insights into pathological and molecular mechanisms. Brain. 143 (1), 303–319.
Igaz, L.M., Kwong, L.K., Chen-Plotkin, A., et al., 2009. Expression of tdp-43 c-terminal fragments in vitro recapitulates pathological features of tdp-43 proteinopathies. J. Biol. Chem. 284 (13), 8516–8524.
Kollmann, K., Uusi-Rauva, K., Scifo, E., Tyynelä, J., Jalanko, A., Braulke, T., 2013. Cell biology and function of neuronal ceroid lipofuscinosis-related proteins. Biochim. Biophys. Acta (BBA) - Mol. Basis Dis. 1832 (11), 1866–1881.
Le Ber, I., Camuzat, A., Hannequin, D., et al., 2008. Phenotype variability in progranulin mutation carriers: a clinical, neuropsychological, imaging and genetic study. Brain. 131 (3), 732–746.
Liu, Y., Ren, J., Kang, M., et al., 2021. Progranulin promotes functional recovery and neurogenesis in the subventricular zone of adult mice after cerebral ischemia. Brain Res. 1757, 147312.
Neumann, M., Mackenzie, I.R.A., 2019. Review: neuropathology of non-tau frontotemporal lobar degeneration. Neuropathol. Appl. Neurobiol. 45 (1), 19–40.
Neumann, M., Kwong, L.K., Lee, E.B., et al., 2009. Phosphorylation of S409/410 of TDP-43 is a consistent feature in all sporadic and familial forms of TDP-43 proteinopathies. Acta Neuropathol. 117 (2), 137–149.
Neuray, C., Sultan, T., Alvi, J.R., et al., 2021. Early-onset phenotype of bi-allelic *GRN* mutations. Brain. 144 (2), e22.
Nita, D.A., Mole, S.E., Minassian, B.A., 2016. Neuronal ceroid lipofuscinoses. Epileptic Disord. 18 (S2), 73–88.
Rissman, R.A., Poon, W.W., Blurton-Jones, M., et al., 2004. Caspase-cleavage of tau is an early event in Alzheimer disease tangle pathology. J. Clin. Invest. 114 (1), 121–130.
Smith, K.R., Damiano, J., Franceschetti, S., et al., 2012. Strikingly different clinicopathological phenotypes determined by progranulin-mutation dosage. Am. J. Hum. Genet. 90 (6), 1102–1107.
Su, J.H., Nichol, K.E., Sitch, T., et al., 2000. Dna damage and activated caspase-3 expression in neurons and astrocytes: evidence for apoptosis in frontotemporal dementia. Exp. Neurol. 163 (1), 9–19.
Tanaka, Y., Matsuwaki, T., Yamanouchi, K., Nishihara, M., 2013. Exacerbated inflammatory responses related to activated microglia after traumatic brain injury in progranulin-deficient mice. Neuroscience. 231, 49–60.
Tao, J., Ji, F., Wang, F., Liu, B., Zhu, Y., 2012. Neuroprotective effects of progranulin in ischemic mice. Brain Res. 1436, 130–136.
Terlizzi, R., Valentino, M.L., Bartoletti-Stella, A., et al., 2017. Muscle ceroid lipofuscin-like deposits in a patient with corticobasal syndrome due to a progranulin mutation: letters: new observations. Mov. Disord. 32 (8), 1259–1260.
Toh, H., Chitramuthu, B.P., Bennett, H.P.J., Bateman, A., 2011. Structure, function, and mechanism of progranulin; the brain and beyond. J. Mol. Neurosci. 45 (3), 538–548.
Valdez, C., Wong, Y.C., Schwake, M., Bu, G., Wszolek, Z.K., Krainc, D., 2017. Progranulin-mediated deficiency of cathepsin D results in FTD and NCL-like phenotypes in neurons derived from FTD patients. Hum. Mol. Genet. 26 (24), 4861–4872.
Valdez, C., Ysselstein, D., Young, T.J., Zheng, J., Krainc, D., 2020. Progranulin mutations result in impaired processing of prosaposin and reduced glucocerebrosidase activity. Hum. Mol. Genet. 29 (5), 716–726.
Van Damme, P., Van Hoecke, A., Lambrechts, D., et al., 2008. Progranulin functions as a neurotrophic factor to regulate neurite outgrowth and enhance neuronal survival. J. Cell Biol. 181 (1), 37–41.
Van Mossevelde, S., Engelborghs, S., van der Zee, J., Van Broeckhoven, C., 2018. Genotype–phenotype links in frontotemporal lobar degeneration. Nat. Rev. Neurol. 14 (6), 363–378.
Ward, M.E., Chen, R., Huang, H.Y., et al., 2017. Individuals with progranulin haploinsufficiency exhibit features of neuronal ceroid lipofuscinosis. Sci. Transl. Med. 9 (385) eaah5642.
Zhang, Y.J., Xu, Y., Dickey, C.A., et al., 2007. Progranulin mediates caspase-dependent cleavage of tar dna binding protein-43. J. Neurosci. 27 (39), 10530–10534.
Zhang, Y.J., Xu, Y.F., Cook, C., et al., 2009. Aberrant cleavage of TDP-43 enhances aggregation and cellular toxicity. Proc. Natl. Acad. Sci. U. S. A. 106 (18), 7607–7612.
Zhou, X., Sun, L., Bastos de Oliveira, F., et al., 2015. Prosaposin facilitates sortilin-independent lysosomal trafficking of progranulin. J. Cell Biol. 210 (6), 991–1002.
Zhou, X., Paushter, D.H., Feng, T., Sun, L., Reinheckel, T., Hu, F., 2017a. Lysosomal processing of progranulin. Mol. Neurodegener. 12 (1), 62.
Zhou, X., Paushter, D.H., Feng, T., Pardon, C.M., Mendoza, C.S., Hu, F., 2017b. Regulation of cathepsin D activity by the FTLD protein progranulin. Acta Neuropathol. 134 (1), 151–153.
Zhou, X., Paushter, D.H., Pagan, M.D., et al., 2019. Progranulin deficiency leads to reduced glucocerebrosidase activity. PLoS One 14 (7), e0212382.